Draft version May 24, 2016
Preprint typeset using LaTeX style emulateapj v. 5/2/11

arXiv:1605.06109v2 [astro-ph.GA] 23 May 2016

FIRST DETECTIONS OF THE KEY PREBIOTIC MOLECULE PO IN STAR-FORMING REGIONS

V. M. Rivilla[1], F. Fontani[1], M. T. Beltrán[1], A. Vasyunin[2,3], P. Caselli[2], J. Martín-Pintado[4], and R. Cesaroni[1]

Draft version May 24, 2016

ABSTRACT

Phosphorus is a crucial element in biochemistry, especially the P−O bond, which is key for the formation of the backbone of the deoxyribonucleic acid. So far, PO has only been detected towards the envelope of evolved stars, and never towards star-forming regions. We report the first detection of PO towards two massive star-forming regions, W51 e1/e2 and W3(OH), using data from the IRAM 30m telescope. PN has also been detected towards the two regions. The abundance ratio PO/PN is 1.8 and 3 for W51 and W3(OH), respectively. Our chemical model indicates that the two molecules are chemically related and are formed via gas-phase ion-molecule and neutral-neutral reactions during the cold collapse. The molecules freeze out onto grains at the end of the collapse and desorb during the warm-up phase once the temperature reaches ∼35 K. Similar abundances of the two species are expected during a period of $\sim 5\times10^4$ yr at the early stages of the warm-up phase, when the temperature is in the range 35−90 K. The observed molecular abundances of 10^{-10} are predicted by the model if a relatively high initial abundance of 5×10^{-9} of depleted phosphorus is assumed.

Subject headings: Stars: formation — ISM: molecules — radio lines: ISM

1. INTRODUCTION

The detection of new interstellar molecules related with prebiotic chemistry in star-forming regions will allow us to make progress on understanding how the building blocks of life could originate in the interstellar medium (ISM). However, there is a key ingredient that still evades detection: phosphorus, P. This element is essential for life (Maciá, Hernández & Oró 1997), because it plays a central role in the formation of P-bearing macromolecules such as phospholipids, which are the structural components of all cellular membranes. Moreover, living cells on Earth use P-bearing compounds, phosphates, to transport energy in the form of adenotryphosphate (ATP; see e.g. Pasek & Lauretta 2005). Especially important to basic biochemistry is the P−O bond, fundamental for many relevant biological molecules such as phosphate esters, which are essential for the formation of the backbone of the genetic macromolecule deoxyribonucleic acid (DNA).

Phosphorus is thought to be synthesized in massive stars and injected to the ISM through supernova explosions (Koo et al. 2013). It is a cosmically relatively abundant element, P/H$\sim 3\times10^{-7}$ (Grevesse & Sauval 1998). It has been detected towards atmospheres of stars (Caffau et al. 2011; Roederer et al. 2014; Caffau et al. 2016), but it is barely detected in the ISM. The ion P^+ has been detected in several diffuse clouds (Jura & York 1978), and only a few simple P-bearing species (PN, PO, CP, HCP, C_2P, PH_3) have been identified towards the circumstellar envelopes of very evolved objects (Tenenbaum, Woolf & Ziurys 2007; De Beck et al. 2013; Agúndez et al. 2014). In star-forming regions, only PN has been detected so far (Turner & Bally 1987; Ziurys & Friberg 1987; Fontani et al. 2016). Previous searches of PO towards star-forming regions (Sutton et al. 1985; Matthews, Feldman & Bernath 1987) were unsuccesful.

Despite the astrobiological importance of P-bearing molecules, their chemistry is still poorly understood in the ISM. The few theoretical models devoted to P-chemistry disagree in both the chemical formation pathways and the predictions of the abundances of PO and PN. While some works (Millar, Bennett & Herbst 1987; Adams, McIntosh & Smith 1990; Charnley & Millar 1994) suggest that PN should be more abundant than PO, other studies involving theoretical modeling and laboratory experiments (e.g. Thorne et al. 1984) predict that P should be found mainly in the form of PO.

To constrain the chemical models and understand the chemistry of phosphorus in the ISM, astronomical detections of PO and PN in star-forming regions are required. We present observations searching for PN and PO towards two massive star-forming regions: the W51 e1/e2 and the W3(OH) complexes (with luminosities of 1.5×10^6 and 1.0×10^5 $L_\odot$, respectively). The W51 star-forming region, located at a distance of 5.1 kpc (Xu et al. 2009) in the Sagittarius arm of our Galaxy, harbors two compact radio sources (Scott 1978) known as e1 and e2, which are associated with hot molecular cores with a rich chemistry (Zhang & Ho 1997; Zhang, Ho & Ohashi 1998; Liu, Mehringer & Snyder 2001; Ikeda et al. 2001; Remijan et al. 2002; Demyk, Wlodarczak & Carvajal 2008; Kalenskii & Johansson 2010; Lykke et al. 2015). The W3(OH) complex, located at 2.04 kpc (Hachisuka et al. 2006), harbors two massive objects separated by 6″: the UC HII region W3(OH) (Wilner, Welch & Forster 1995) and the chemically rich $W3(H_2O)$ hot molecular core (Wyrowski et al. 1999; Zapata et al. 2011; Qin et al. 2015).

In this paper, we report the first detection of PO towards these two massive star-forming regions.

[1] Osservatorio Astrofisico di Arcetri, Largo Enrico Fermi 5, I-50125, Firenze, Italia
[2] Max-Planck Institute for Extraterrestrial Physics, Giessenbachstrasse 1, 85748, Garching, Germany
[3] Ural Federal University, Ekaterinburg, Russia
[4] Centro de Astrobiología (CSIC-INTA), Ctra. de Torrejón a Ajalvir km 4, 28850, Torrejón de Ardoz, Madrid, Spain

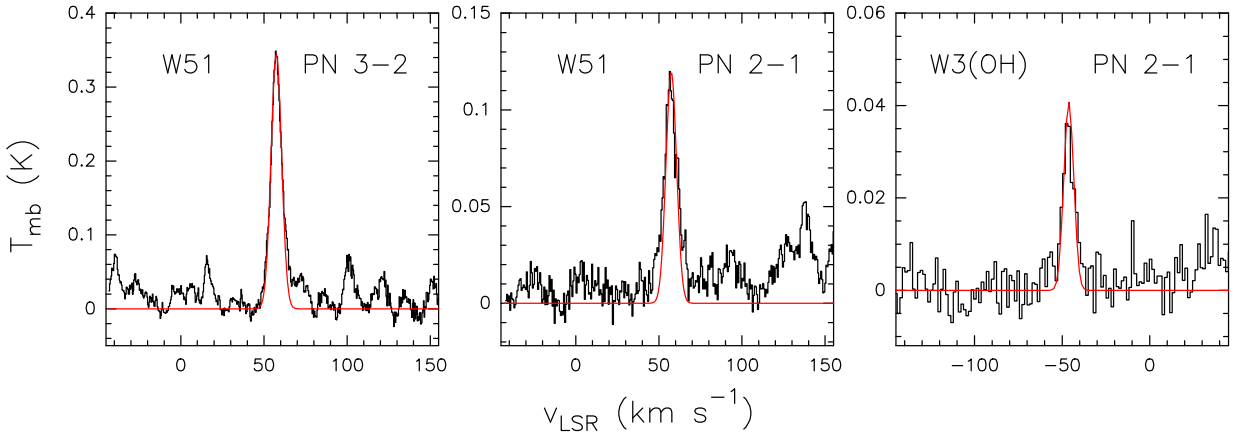

FIG. 1.— PN transitions observed towards W51 and W3(OH). The red line is the LTE fit for a excitation temperature of 35 K (see text), and the source-average column densities given in Table 3.

TABLE 1
SUMMARY OF THE IRAM 30M OBSERVATIONS TOWARDS THE W51 AND W3(OH) HOT MOLECULAR CORES.

Date	Source	RA_{J2000}	DEC_{J2000}	Frequency coverage (GHz)
2012 Apr 25	W51	$19h\ 23m\ 43.90s$	$14°\ 30'\ 32.0''$	88.83-96.60 &
	W3(OH)	$2h\ 27m\ 04.69s$	$61°\ 52'\ 25.51''$	104.51-112.29
2012 Dec 13	W51	$19h\ 23m\ 43.90s$	$14°\ 30'\ 34.8''$	99.70-106.30 &
				238.20-245.98
2015 Dec 9	W51	$19h\ 23m\ 43.90s$	$14°\ 30'\ 32.0''$	134.47-142.25 &
				150.15-157.90

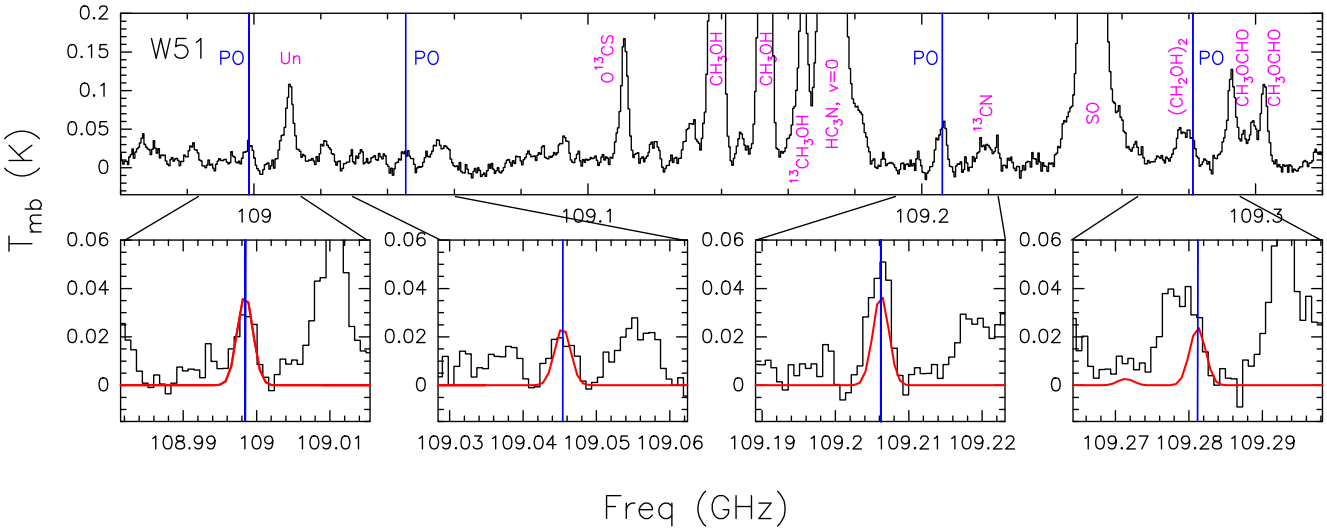

FIG. 2.— Spectrum observed at 3 mm towards W51. The PO transitions are indicated with blue vertical lines. The lower panels show zoom-in views of the PO transitions. The red line is the LTE fit with a excitation temperature of 35 K and an assumed source size of 20″ (see text).

2. OBSERVATIONS

We used data from different observing runs performed with the IRAM 30m telescope at Pico Veleta (Spain) on 2012 and 2015[5]. The dates, positions and frequency coverage of these observations are summarized in Table 1. The W51 e1/e2 (hereafter W51) region was observed at 1, 2 and 3 mm, while the W3(OH) region was observed at 3 mm.

All observing campaigns used the Eight Mixer Receiver (EMIR) and the Fast Fourier Transform Spectrometer (FTS), which provides a spectral resolution of 0.195 kHz. The spectra were exported from the software package CLASS of GILDAS[6] to MADCUBAIJ[7], which was

[5] The Dec 2012 data were obtained from Lykke et al. (2015).

[6] The GILDAS software is available at http://www.iram.fr/IRAMFR/GILDAS

[7] Madrid Data Cube Analysis on ImageJ is a software developed

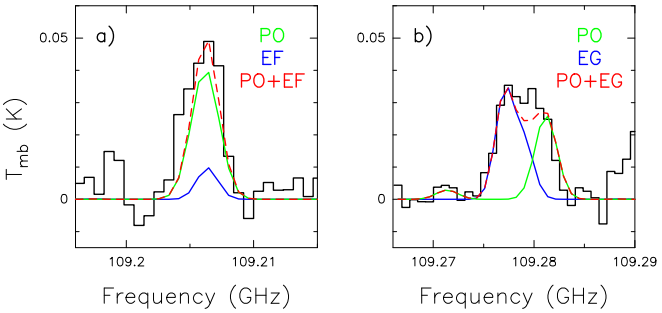

FIG. 3.— Simultaneous LTE fit of the PO transitions at 109.206 GHz and 109.281 GHz and transitions of ethyl formate (EF) and ethylene glycol (EG) that are partially blended.

used for the line identification and analysis. The line intensity of the IRAM 30m spectra was converted to the main beam temperature T_{mb} scale, using the efficiencies provided by IRAM[8]. The half-power beam widths of the observations can be estimated using the expression $\theta_{\rm beam}[{\rm arcsec}]=2460/\nu({\rm GHz})$.

3. RESULTS

3.1. *Detection of PN*

We have detected the J=2−1 and J=3−2 transitions of PN (Table 2) towards W51 (left and middle panels of Fig 1). This molecule was already detected towards this source by Turner & Bally (1987) using the NRAO 12m telescope. The comparison of the line intensities of the PN J=2−1 transition observed with the 30m and 12m telescopes towards W51 allows us to estimate the size of the PN emission. The approximate size of the emitting region, θ_s, can be estimated from the expression:

$$T_{\rm 12m}\frac{\theta_{\rm s}^2+\theta_{\rm 12m}^2}{\theta_{\rm s}^2}=T_{\rm 30m}\frac{\theta_{\rm s}^2+\theta_{\rm 30m}^2}{\theta_{\rm s}^2}, \qquad (1)$$

where $\theta_{\rm 12m}$=69″ and $\theta_{\rm 30m}$=26″ are the HPBW of the two telescopes, $T_{\rm 12m}$=20 mK and $T_{\rm 30m}$=120 mK are the corresponding main-beam brightness temperatures. We obtain an angular size of the emitting region of ∼12″. Using this angular diameter, the LTE simulated spectra reproduce the PN J=2−1 and J=3−2 transitions for an excitation temperature of ∼35 K (Fig. 1), as previously found by Turner & Bally (1987). We derived a PN source-averaged column density of 2.1×10^{13} cm^{-2} (Table 3). Using the derived H_2 column density $N_{\rm H_2}$ (see the details of the calculation in Appendix A), the molecular abundance with respect to molecular hydrogen is 1.1×10^{-10}.

We have also detected the J=2−1 PN transition towards W3(OH) (right panel of Fig. 1). To our knowledge this is the first detection of PN towards this source. Assuming the same excitation temperature and linear diameter as that of W51 (i.e. 30″ at the distance of W3(OH)), we obtained a source-averaged PN column density of 0.2×10^{13} cm^{-2}, which implies a molecular abundance of 0.4×10^{-10}.

3.2. *Detection of PO*

in the Center of Astrobiology (Madrid, INTA-CSIC) to visualize and analyze single spectra and datacubes (Martín et al., *in prep.*).

[8] http://www.iram.es/IRAMES/mainWiki/Iram30mEfficiencies

TABLE 2
SPECTROSCOPIC PARAMETERS OF TARGETED PN TRANSITIONS, FROM CDMS.

Frequency (GHz)	Transition	$S_{ij}\mu^2$ (D^2)	E_{up} (K)
93.97977	2−1	15.1	6.8
140.96769	3−2	22.6	13.5

TABLE 3
PHYSICAL PARAMETERS OF PO AND PN FROM THE LTE ANALYSIS.

Molecule	Source	$T_{\rm ex}$ (K)	$N_{\rm s}$ ($\times10^{13}$ cm^{-2})	$N_{\rm b}$	$v_{\rm LSR}$ (km s^{-1})	Δv (km s^{-1})	$X_{\rm s}$ (10^{-10})
PN	W51	35	2.1	0.4	57.5	8.2	1.1
	W3(OH)	35	0.2	0.13	-46.2	6.6	0.4
PO	W51	35	4.0	0.7	57.0	7.0	2.0
	W3(OH)	35	0.6	0.3	-46.2	6.6	1.2

Note: $T_{\rm ex}$ (excitation temperature), N_s (source averaged column density), N_b (beam averaged column density), $v_{\rm LSR}$ (central velocity of the molecular emission), Δv (molecular linewith, i.e. the full width half maximum of the line gaussian profile), $X_{\rm s}$ (source averaged molecular abundances).

TABLE 4
SPECTROSCOPIC PARAMETERS OF TARGETED PO TRANSITIONS ($S_{ij}\mu^2$ > 5 D^2 AND E_{up} (K) < 300 K), FROM CDMS.

Frequency (GHz)	Transition	$S_{ij}\mu^2$ (D^2)	E_{up} (K)
J=5/2−3/2, Ω=1/2			
108.99845	F=3−2, l=e	9.9	8.4
109.04540	F=2−1, l=e	6.4	8.4
109.20620	F=3−2, l=f	9.9	8.4
109.28119	F=2−1, l=f	6.4	8.4
J=7/2−5/2, Ω=1/2			
152.65698	F=4−3, l=e	13.6	15.7
152.68028	F=3−2, l=e	10.1	15.7
152.85545	F=4−3, l=f	13.6	15.7
152.88813	F=3−2, l=f	10.1	15.7
J=11/2−9/2, Ω=1/2			
239.94898	F=6−5, l=e	20.9	36.7
239.95810	F=5−4, l=e	17.4	36.7
240.14106	F=6−5, l=f	20.9	36.7
240.15253	F=5−4, l=f	17.4	36.7

The PO radical is a diatomic molecule with a dipole moment of μ=1.88 D (Kanata, Yamamoto & Saito 1988). Its millimeter spectrum was measured in the gas phase in the laboratory by Kawaguchi, Saito & Hirota (1983). PO has a $^2\Pi_{\rm r}$ ground electronic state, and therefore each J-transition splits into a doublet because of Λ coupling. The spin of I=1/2 of the phosphorus atom produces a further splitting of each Λ doublet into two hyperfine levels. Table 4 shows the PO transitions that are most likely detectable in the ISM with the 30m telescope: the brightest transitions of the Ω=1/2 ladder, with $S_{ij}\mu^2$ > 5 D^2, and with energy levels E_{up} < 300 K. The lower energy (E_{up}= 3 K) and lower frequency transitions (J=3/2−1/2) at 65 GHz of the Ω=1/2 ladder are not observable due to atmospheric opacity. The J=9/2−7/2 quadruplet falls at 196 GHz, out of the range covered by the IRAM 30m telescope. The search for

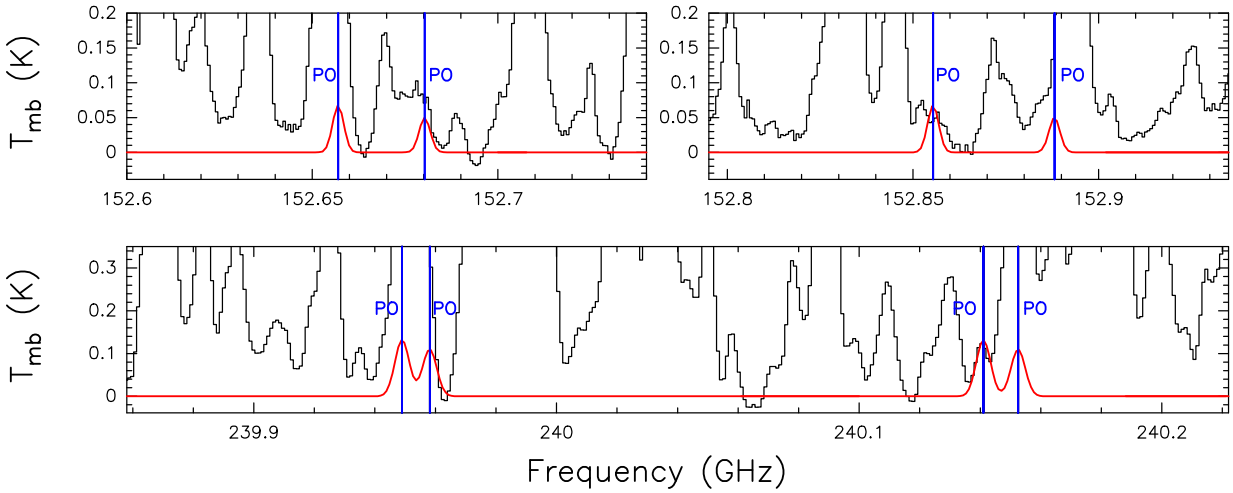

FIG. 4.— PO transitions at 1 and 2 mm observed towards the W51 hot core. The PO transitions are indicated with blue vertical lines and the red line is the LTE fit as in Fig. 2.

higher energy PO transitions (e.g. J=13/2−11/2 at 283 GHz) is much less feasible, due to strong contamination from brighter molecular lines at this frequency. Therefore, the PO transitions given in Table 4 are the best candidates for a detection. The observations towards W51 covered all these PO transitions (at 1, 2 and 3 mm), while the observations towards W3(OH) only covered the 3 mm transitions.

We have used MADCUBAIJ to identify the PO transitions in the observed spectra. We have assumed the same temperature (T_{ex}=35 K) and source size as that of PN to produce the LTE spectrum. We show the 3 mm spectra of W51 and the LTE fit in Fig. 2. We have clearly identified the PO quadruplet towards W51. The four transitions are well fitted by the LTE model. The lines are detected above 6σ. We note that these PO transitions have already been detected in the wind of the oxygen-rich AGB star IK Tauri by De Beck et al. (2013).

The PO transitions at 108.99845 GHz and 109.04540 GHz are completely free of contamination. The transition at 109.20620 GHz also seems unblended, although the LTE model slightly underestimates the observed intensities. The transition at 109.28119 GHz appears clearly blended with another species. To firmly confirm the detection of PO, we have evaluated the possibility of contamination from lines of other molecules. We have searched in the available catalogs (CDMS[9] and JPL[10]) and conclude that there are no transitions blended with the PO lines at 108.99845 GHz and 109.04540 GHz. The only possible contaminantion of the PO transition at 109.20620 GHz is the complex organic molecule ethyl formate, C_2H_5OCHO. Interestingly, this molecule has been recently identified towards W51 (Rivilla et al., *submitted*) based on the detection of multiple transitions, which has allowed us to derive its rotational temperature and column density. Using the physical parameters derived in Rivilla et al. (*submitted*) (N=$10^{16.3}$, T =100 K), we have predicted the LTE line profile of the ethyl formate transition close to the 109.20620 GHz transition of PO. The result is shown in the left panel of Fig. 3. Ethyl formate has a very weak contribution to the observed emission, which is hence mainly due to PO. The LTE profile reproduces very well the observed line profile if the emission of both molecules is taken into account (see left panel of Fig. 3).

In the case of the 109.28119 GHz transition of PO, we have found that it is blended with a line of ethylene glycol, $(CH_2OH)_2$. This species has been tentatively identified towards W51 by Lykke et al. (2015) from observations at 1 mm. Our 2 and 3 mm spectra clearly confirm the detection of ethylene glycol, and allow us to confirm the excitation temperature of ∼120 K previously obtained by Lykke et al. (2015). We show in the right panel of Fig. 3 the LTE model of the ethylene glycol transition close to the 109.28119 GHz transition of PO. The combined contribution of PO and ethylene glycol reproduces well the observed spectral line profile.

The LTE fit of the four PO spectral features at 3 mm gives a source-averaged PO column density of 4×10^{13} cm^{-2} and a molecular abundance of 2×10^{-10} (Table 3). In Fig. 4 we also show the predicted LTE lines profile of the PO at 1 and 2 mm (Table 4). The LTE prediction is consistent with the observed spectra. The predicted PO transition at 240.14106 GHz fits a partially blended line of the observed spectrum (Fig. 4), while the other PO transitions appear heavily blended with brighter lines of other molecular species. In summary, we have detected all the 12 detectable PO transitions towards W51 with intensities consistent with LTE emission: two of them (at 3 mm) are unblended, two (at 3 mm) are partially blended, while the others (all the 2 mm and 1 mm transitions) are heavily blended.

For W3(OH), we show in Fig. 5 the observed 3 mm spectra. The two brightest lines of PO (108.99845 GHz and 109.20620 GHz) are detected at a $\sim 4\sigma$ level. We have fitted these lines with the LTE model, assuming T_{ex}=35 K and the same diameter assumed for PN (30″), and obtained a column density of 0.6×10^{13} cm^{-2} and a molecular abundance of 1.2×10^{-10} (Table 3). To confirm this detection we have stacked the 3 mm observed spectra to improve the signal to noise ratio. This method is used to identify molecular species marginally detected in several lines. In practice, we have averaged the observed spectra of the 4 PO transitions with the weights calculated assuming LTE, and normalized the result to

[9] http://www.astro.uni-koeln.de/cdms
[10] http://spec.jpl.nasa.gov/

the peak value. The resulting spectrum, shown in Fig. 6, indicates a clear detection at the systemic velocity of the source. The signal is $> 5\sigma$, confirming the detection of PO towards W3(OH).

4. DISCUSSION: THE CHEMISTRY OF PHOSPHORUS

4.1. *The PO/PN ratio*

The LTE fits of PO and PN transitions show that the molecular abundances of the two molecules are similar in the two sources ($\sim 10^{-10}$), being the PO abundance higher by a factor $\sim$2. Our detections towards W51 and W3(OH) show that the line intensities of PO at 3 mm are a factor $\geq$4 weaker than the PN J=2−1 transition at similar wavelengths. This makes the identification of PO more difficult than that of PN and explains why previous attempts to detect PO were fruitless. Matthews, Feldman & Bernath (1987) derived upper limits of the beam averaged column densities[11] of four hot molecular cores of $< (0.2-2.7)\times 10^{13}$ cm^{-2}. These upper limits are consistent with the PO column densities we have derived, suggesting that the non-detections of Matthews, Feldman & Bernath (1987) were due to insufficient sensitivity.

More recently, Fontani et al. (2016) have found upper limits for the PO/PN ratio of $< (1.3-4.5)$ towards a sample of massive star-forming cores (see Table 5), which are also consistent with the abundances of both P-bearing species estimated by us. The upper limit of the PO/PN ratio of $\sim$0.5−1.3 found towards a protostellar shock by Aota & Aikawa (2012) is also in agreement with our observed ratios.

Before the present detections, PO had only been detected towards the envelopes of two evolved stars, VY Canis Majoris (Tenenbaum, Woolf & Ziurys 2007), and IK Tauri (De Beck et al. 2013), where the PO/PN ratios are 2.2 and 0.17−2, respectively. These ratios are similar to those found towards W51 and W3(OH), suggesting that phosphorus seems to be equally distributed in the form of PO and PN in both interstellar and circumstellar material.

4.2. *Chemical model: constraining the phosphorus chemistry*

We have investigated the formation of the phosphorus-bearing molecules PO and PN in massive star-forming regions using the model based on Vasyunin & Herbst (2013), which simulates the chemical evolution of a parcel of gas and dust with time-dependent physical conditions. First, the formation of a dark dense clump from a translucent cloud during free-fall collapse is simulated (″cold starless phase ″). During this phase, the density increases from 10^3 cm^{-3} to 10^6 cm^{-3} and visual extinction rises from A_v=2 to $A_v \gg$100 mag. Gas and dust temperatures are both decreasing slightly from 20 K to 10 K. On a second phase, the dense dark clump warms up from 10 K to 200 K during 2×10^5 years, thus developing into a hot core (″warm-up protostellar phase ″). We have defined as time 0 the moment when the protostar starts to heat up the environment.

We used two sets of initial chemical abundances to explore the influence of the poorly constrained P depletion factor: i) the ″low metals ″ model (EA1, see Table 1 in Wakelam & Herbst 2008), where the atomic P is depleted and has an abundance of 2×10^{-10} with respect to hydrogen, typically used in dark cloud chemical models; and ii) the ″high metals ″ model, where the phosphorus abundance is increased by a factor of $\sim$25 to 5×10^{-9}.

The results of the modeling are shown in Fig. 7, which shows the temporal evolution of the temperature (Fig. 7a), gas abundance of water (Fig. 7b), gas abundances of PO and PN (Fig. 7c) and the PO/PN ratio (Fig. 7d). The two P-bearing species are chemically related and are formed purely in a sequence of gas-phase ion-molecule and neutral-neutral reactions. PO is efficiently formed during the cold collapse phase in a sequence of reactions:

$$H_3O^+ + P \longrightarrow HPO^+ + H_2 \quad (2)$$

$$HPO^+ + e^- \longrightarrow PH + O \quad (3)$$

$$HPO^+ + e^- \longrightarrow PO + H \quad (4)$$

$$P^+ + H_2 \longrightarrow PH_2^+ \quad (5)$$

$$PH_2^+ + e^- \longrightarrow PH + H \quad (6)$$

$$O + PH \longrightarrow PO + H \quad (7)$$

PN is mainly formed from PO via:

$$N + PO \longrightarrow PN + O \quad (8)$$

During the starless phase the model predicts that PO is more abundant than PN (Fig. 7c). Both species freeze out to grains at the end of the cold collapse phase and

TABLE 5
Column densities and relative abundances of PO and PN in different sources.

Source	N_{PN}	N_{PO}	N_{PO}/N_{PN}	Ref.
	Star-forming regions			
	$\times 10^{11}$ cm^{-2}	$\times 10^{11}$ cm^{-2}		
W51 e1/e2	210	400	1.8	(1)
W3(OH)	20	60	3.0	(1)
AFGL5142-EC[a]	8.3	< 20	< 2.4	(2)
05358−mm3[a]	2.9	< 13	< 4.5	(2)
AFGL5142−MM[a]	6.9	< 12	< 1.7	(2)
18089−1732[a]	3.3	< 6.3	< 1.9	(2)
18517−0437[a]	2.0	< 4.4	< 2.2	(2)
G5.89-0.39[a]	10.4	< 14	< 1.3	(2)
19410+2336[a]	1.6	< 3.3	< 2.0	(2)
ON1[a]	3.8	< 6.3	< 1.7	(2)
	Protostellar shocks			
L1157 B1[a]	4.2−11	< 5.3	$< 0.5-1.3$	(3)
	Envelopes of evolved stars			
	$\times 10^{15}$ cm^{-2}	$\times 10^{15}$ cm^{-2}		
VY Canis Majoris	1.2	2.8	2.2	(4)
IK Tauri	2.2	0.4−4.4	0.17−2	(5)

[a] Beam-averaged column densities.
References: (1) This paper; (2) Fontani et al. (2016); (3) Aota & Aikawa (2012); (4) Tenenbaum, Woolf & Ziurys (2007); (5) De Beck et al. (2013).

[11] Matthews, Feldman & Bernath (1987) derived the PO upper limits assuming a dipole moment of PO of 2.13 Debye. Kanata, Yamamoto & Saito (1988) measured a dipole moment of 1.88, so we have corrected the PO upper limits of Table 1 of Matthews, Feldman & Bernath (1987) by multiplying for a factor $(2.13/1.88)^2 \simeq 1.3$.

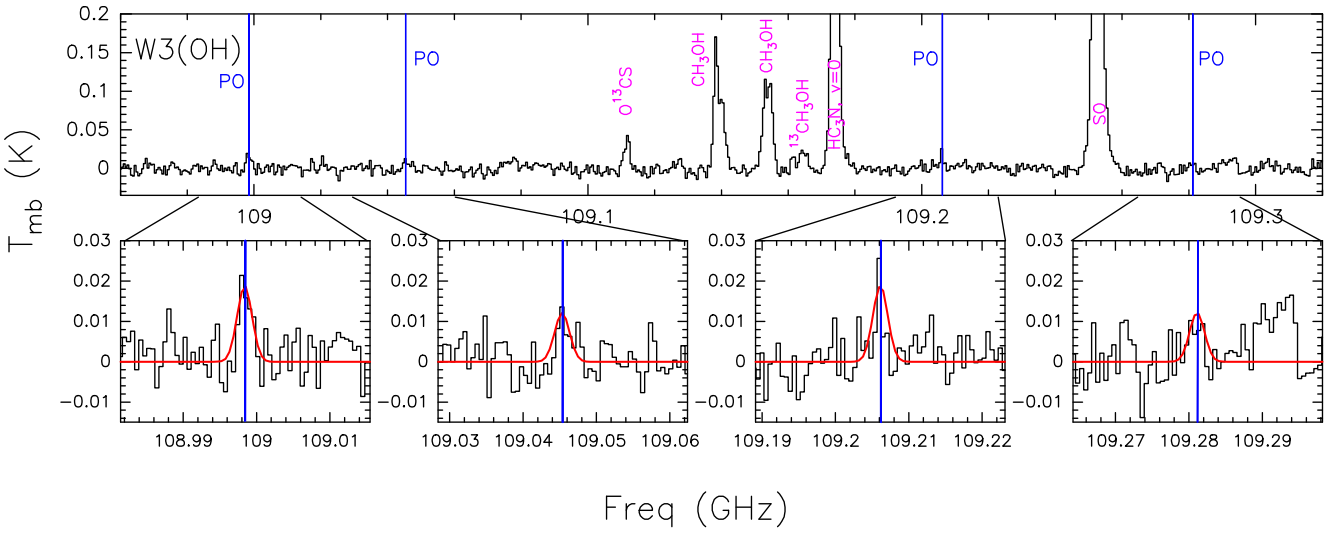

FIG. 5.— Same as Fig. 2 for the W3(OH) hot core.

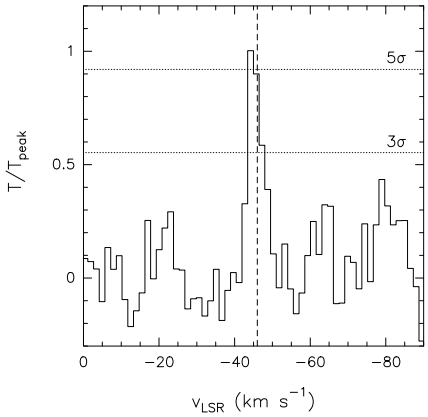

FIG. 6.— Composite normalized spectrum of PO towards W3(OH). The dashed vertical line indicates the systemic velocity of the source, while the dotted horizontal lines show the 3σ and 5σ detection levels.

consequently the gas abundances sharply decrease (Fig. 7c). PO has an abundance ∼5 times higher than PN at that time.

At the warm-up phase, once the temperature gradually increases from 10 K to 200 K (Fig. 7a), the species evaporate to the gas phase in the order determined by their desorption energies. PO and PN desorb simultaneously when the temperature reaches ∼35 K (∼0.7×10^5 yr, Fig. 7c), because in our model they have the same evaporation energy of 1900 K[12].

Some PO is converted to PN via gas-phase reactions, and the abundances of the two species become almost equal until ∼1.2×10^5 yr (Fig. 7c). Once the temperature reaches ∼100 K, water ice evaporates and the gas-phase abundance of water reaches a high value of 10^{-4} (see Fig. 7b). Then, the abundance of protonated water H_3O^+ correspondingly increases, and PN reacts with H_3O^+:

$$PN + H_3O^+ \longrightarrow HPN^+ + H_2O \quad (9)$$

In turn, HPN^+ has two equally probable channels of dissociative recombination:

$$HPN^+ + e^- \longrightarrow PN + H \quad (10)$$

$$HPN^+ + e^- \longrightarrow PH + N \quad (11)$$

Since the abundance of atomic oxygen is higher by almost an order of magnitude than the abundance of atomic nitrogen, PH is preferrably converted to PO rather than PN. As such, PN is gradually destroyed, while PO is additionally produced, which significantly increases the PO/PN ratio (Fig. 7d).

To compare the results of the observations with the predictions of our chemical models, we show the values of the abundances and the PO/PN ratio derived from the observations (Table 3) in Figs. 7c and 7d, respectively. The main source of uncertainty of the estimated abundances arises from the uncertainty of the size of the emmiting region and the H_2 column density. We have considered a conservative range of one order of magnitude uncertainty for the abundances, i.e. $(0.5-5)\times10^{-10}$ (see Fig. 7c). In the case of the PO/PN ratio, which is independent of the H_2 column density, we have considered a lower uncertainty of a factor of 5, i.e., values in the range 1−5. These observational constraints can only be explained by the "high metals" model (Fig. 7c), and during a period of ∼5×10^4 yr (between 0.8 and 1.2×10^5 yr in Fig. 7). This suggests that the value of the initial depleted atomic abundance of P is a factor of ∼25 higher (i.e. 5×10^{-9}) than that commonly assumed by the standard "low metal" model.

The temporal window that fulfills the observational constraints translates in a temperature range between the desorption temperature of the P-bearing molecules (35 K) and ∼90 K (see Fig. 7a). The former temperature is the same than that derived from PN transitions towards W51, which may indicate that the observations have detected the bulk of PN (and PO) that have recently desorbed from dust grains. The latter temperature is just below the sublimation temperature of the bulk of water (100 K), when PN is efficiently destroyed and partially converted to PO. Then, the gas abundace of water predicted by the model at this stage is still low, ∼10^{-9}, which is in good agreement with the values of

[12] To the best of our knowledge, there are no experimental data on PN and PO desorption energies, and therefore, the results of the modeling should be accepted with some caution.

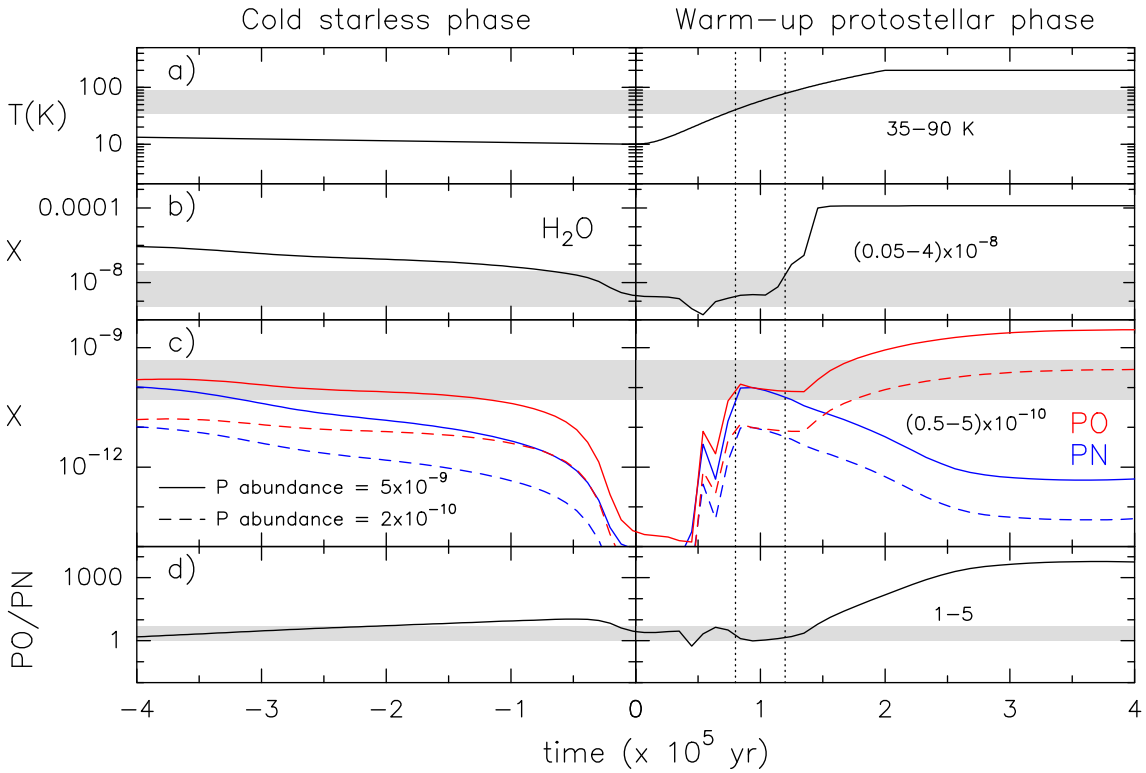

FIG. 7.— Results of our chemical model. The left panels correspond to the cold collapse phase, and the right panels to the subsequent warm-up phase. We show the evolution during 0.8×10^5 yr, being time 0 the moment when the protostar starts to heat up the environment. The two vertical dotted lines in the right panels indicate the temporal range for which the observational constraints are fulfilled (see text). *a)* Evolution of the temperature assumed by the model. The grey band corresponds to the temperature range between 35 and 90 K which is compatible with the observational constraints (see text). *b)* H_2O abundance. The grey band corresponds to the range found towards massive star-forming regions by Marseille et al. (2010). *c)* PO and PN abundances predicted by the model (red and blue lines, respectively). We have considered two different initial abundances of depleted atomic phosphorus: 5×10^{-9} (solid lines, "high metals" model), and 2×10^{-10} (dashed lines, "low metals" model, usually assumed in dark cloud models). The grey band indicates a conservative range of one order of magnitude around the molecular abundances derived from our observations of PO and PN (see text). *d)* Ratio of the molecular abundances of PO and PN. The grey band shows a conservative range (1−5) around the ratio found by the observations.

5×10^{-10} − 4×10^{-8} found towards several massive star-forming regions by Marseille et al. (2010) (see Fig. 7b).

5. SUMMARY AND CONCLUSIONS

We report on the first detection of the key prebiotic molecule PO towards two star-forming regions: W51 e1/e2 and W3(OH). The derived molecular abundances of PO are $\sim10^{-10}$ in both sources. We have found an abundance ratio PO/PN of 1.8 and 3 for W51 e1/e2 and W3(OH), respectively, in agreement with the values estimated for evolved stars. Our chemical modelling indicates that the two molecules are chemically related and are formed via gas-phase ion-molecular and neutral-neutral reactions during the cold collapse. The molecules freeze out onto grains at the end of the collapse, and evaporate during the warm-up phase once the temperature reach ∼35 K. Similar abundances of PO and PN are expected during a period of $\sim5\times10^4$ yr at the early stages of the warm-up phase, when the temperature is in the range 35−90 K. The observed molecular abundances require a relatively high initial abundance of depleted atomic phosphorus of 5×10^{-9}, 25 times higher than the "low metal" P-abundance typically used in dark cloud chemical models.

ACKNOWLEDGMENTS

The authors are grateful to the IRAM staff for its help during the observations of the IRAM 30m data, and especially to the Director for allowing us to use the telescope time during the DDT proposal D04−15. This work was partly supported by the Italian Ministero dell'Istruzione, Università e Ricerca through the grant Progetti Premiali 2012 − iALMA. PC and AV acknowledge the financial support of the European Research Council (ERC; project PALs 320620). JM-P acknowleges partial support by the MINECO under grants AYA2010-2169-C04-01, FIS2012-39162-C06-01, ESP2013-47809-C03-01 and ESP2015-65597-C4-1.

REFERENCES

Adams N. G., McIntosh B. J., Smith D., 1990, A&A, 232, 443
Agúndez M., Cernicharo J., Decin L., Encrenaz P., Teyssier D., 2014, ApJ, 790, L27
Aota T., Aikawa Y., 2012, ApJ, 761, 74
Caffau E., Andrievsky S., Korotin S., Origlia L., Oliva E., et al., 2016, A&A, 585, A16
Caffau E., Bonifacio P., Faraggiana R., Steffen M., 2011, A&A, 532, A98

Charnley S. B., Millar T. J., 1994, MNRAS, 270, 570
Csengeri T., Urquhart J. S., Schuller F., Motte F., Bontemps S., et al., 2014, A&A, 565, A75
De Beck E., Kamiński T., Patel N. A., Young K. H., Gottlieb, et al., 2013, A&A, 558, A132
Demyk K., Wlodarczak G., Carvajal M., 2008, A&A, 489, 589
Di Francesco J., Johnstone D., Kirk H., MacKenzie T., Ledwosinska E., 2008, ApJS, 175, 277
Fontani F., Rivilla V. M., Caselli P., Vasyunin A., Palau A., 2016, ArXiv e-prints:1604.02565, accepted in ApJ
Grevesse N., Sauval A. J., 1998, SSRv, 85, 161
Hachisuka K., Brunthaler A., Menten K. M., Reid M. J., Imai H., et al., 2006, ApJ, 645, 337
Ikeda M., Ohishi M., Nummelin A., Dickens J. E., Bergman P., et al., 2001, ApJ, 560, 792
Jura M., York D. G., 1978, ApJ, 219, 861
Kalenskii S. V., Johansson L. E. B., 2010, ARep, 54, 1084
Kanata H., Yamamoto S., Saito S., 1988, JMoSp, 131, 89
Kawaguchi K., Saito S., Hirota E., 1983, J. Chem. Phys.
Koo B.-C., Lee Y.-H., Moon D.-S., Yoon S.-C., Raymond J. C., 2013, Science, 342, 1346
Liu S.-Y., Mehringer D. M., Snyder L. E., 2001, ApJ, 552, 654
Lykke J. M., Favre C., Bergin E. A., Jørgensen J. K., 2015, A&A, 582, A64
Maciá E., Hernández M. V., Oró J., 1997, OrLi, 27, 459
Marseille M. G., van der Tak F. F. S., Herpin F., Wyrowski F., Chavarría L., et al., 2010, A&A, 521, L32
Matthews H. E., Feldman P. A., Bernath P. F., 1987, ApJ, 312, 358
Millar T. J., Bennett A., Herbst E., 1987, MNRAS, 229, 41P
Ossenkopf V., Henning T., 1994, A&A, 291, 943
Pasek M. A., Lauretta D. S., 2005, AsBio, 5, 515
Qin S.-L., Schilke P., Wu J., Wu Y., Liu T., et al., 2015, ApJ, 803, 39
Remijan A., Snyder L. E., Liu S.-Y., Mehringer D., Kuan Y.-J., 2002, ApJ, 576, 264
Roederer I. U., Jacobson H. R., Thanathibodee T., Frebel A., Toller E., 2014, ApJ, 797, 69
Scott P. F., 1978, MNRAS, 183, 435
Sutton E. C., Blake G. A., Masson C. R., Phillips T. G., 1985, ApJS, 58, 341
Tenenbaum E. D., Woolf N. J., Ziurys L. M., 2007, ApJ, 666, L29
Thorne L. R., Anicich V. G., Prasad S. S., Huntress, Jr. W. T., 1984, ApJ, 280, 139
Turner B. E., Bally J., 1987, ApJ, 321, L75
Vasyunin A. I., Herbst E., 2013, ApJ, 762, 86
Wakelam V., Herbst E., 2008, ApJ, 680, 371
Wilner D. J., Welch W. J., Forster J. R., 1995, ApJ, 449, L73
Wyrowski F., Schilke P., Walmsley C. M., Menten K. M., 1999, ApJ, 514, L43
Xu Y., Reid M. J., Menten K. M., Brunthaler A., Zheng X. W., et al., 2009, ApJ, 693, 413
Zapata L. A., Rodríguez-Garza C., Rodríguez L. F., Girart J. M., Chen H.-R., 2011, ApJ, 740, L19
Zhang Q., Ho P. T. P., 1997, ApJ, 488, 241
Zhang Q., Ho P. T. P., Ohashi N., 1998, ApJ, 494, 636
Ziurys L. M., Friberg P., 1987, ApJL, 314, L49

APPENDIX

CALCULATION OF THE HYDROGEN COLUMN DENSITY

One can derive the hydrogen column density of a clump from the continuum flux emitted by the dust. Assuming an homogeneous clump with temperature $T_{\rm d}$ and opacity τ_ν at frequency ν, the solution of the radiative transfer equation gives the intensity emitted:

$$I_\nu = B_\nu(T_{\rm d})(1 - e^{-\tau_\nu}), \tag{A1}$$

where B_ν is the Plank function:

$$B_\nu = \frac{2h\nu^3}{c^2}\frac{1}{e^{h\nu/kT_{\rm d}} - 1}, \tag{A2}$$

where c is the speed of light, k is the Boltzmann's contant, and h is the Plank's constant.

One can relate the flux density measured within the beam solid angle of the telescope (Ω) with the intensity using:

$$I_\nu = \frac{F_\nu}{\Omega}. \tag{A3}$$

Combining eqs. A1 and A3, one can derive the opacity of the dust emission inside the beam:

$$\tau_\nu = -\ln\left(1 - \frac{F_\nu}{\Omega\ B_\nu(T_d)}\right). \tag{A4}$$

Since the opacity is defined as:

$$\tau_\nu = \int \kappa_\nu\ \rho\ dr, \tag{A5}$$

where ρ is the volume density and κ_ν is the absorption coefficient per unit density, one can derive the hydrogen column density with the optical depth using:

$$N_{H_2} = \int \frac{\rho}{\mu\ m_{\rm H}}\ dr = \frac{\tau_\nu}{\mu\ m_{\rm H}\ \kappa_\nu}, \tag{A6}$$

where $m_{\rm H}$ is the hydrogen mass and μ=2.8 is the mean molecular mass of the ISM with respect to H_2 molecules. We have used eqs. A4 and A6 to derive the dust opacity and the hydrogen colum density of W51 and W3(OH) from the dust continuum emission from ATLASGAL (870 μm, Csengeri et al. 2014) and SCUBA (850 μm, Di Francesco et al. 2008) surveys, respectively. We have considered that the dust temperature is the same as the excitation temperature derived for PN, 35 K. We have adopted a gas-to-dust ratio of 100 and κ_ν=1.85 cm^2 g^{-1}, from interpolation of the

TABLE 6
Continuum fluxes of W51 e1/e2 and W3(OH) clumps from ATLASGAL and SCUBA, respectively, and derived dust opacities and molecular hydrogen column densities.

Source	λ (μm)	F_ν (Jy beam^{-1})	τ	$N_{\rm H_2}$ ($\times 10^{23}$ cm^{-2})
W51	870	70.2[a]	0.02	2.0
W3(OH)	850	26.3[b]	0.005	0.5

[a] From ATLASGAL (Csengeri et al. 2014); [b] From SCUBA (Di Francesco et al. 2008).

column 5 of Table 1 of Ossenkopf & Henning (1994). We have used the peak flux densities shown in Table 6, and the corresponding telescope beams: 19.2″ (ATLASGAL) and 22.9″ (SCUBA). The results are given in Table 6. We have used the values of $N_{\rm H_2}$ to compute the molecular abundances of PN and PO (see Table 3).

REFERENCES

Adams N. G., McIntosh B. J., Smith D., 1990, A&A, 232, 443
Agúndez M., Cernicharo J., Decin L., Encrenaz P., Teyssier D., 2014, ApJ, 790, L27
Aota T., Aikawa Y., 2012, ApJ, 761, 74
Caffau E., Andrievsky S., Korotin S., Origlia L., Oliva E., et al., 2016, A&A, 585, A16
Caffau E., Bonifacio P., Faraggiana R., Steffen M., 2011, A&A, 532, A98
Charnley S. B., Millar T. J., 1994, MNRAS, 270, 570
Csengeri T., Urquhart J. S., Schuller F., Motte F., Bontemps S., et al., 2014, A&A, 565, A75
De Beck E., Kamiński T., Patel N. A., Young K. H., Gottlieb, et al., 2013, A&A, 558, A132
Demyk K., Wlodarczak G., Carvajal M., 2008, A&A, 489, 589
Di Francesco J., Johnstone D., Kirk H., MacKenzie T., Ledwosinska E., 2008, ApJS, 175, 277
Fontani F., Rivilla V. M., Caselli P., Vasyunin A., Palau A., 2016, ArXiv e-prints:1604.02565, accepted in ApJ
Grevesse N., Sauval A. J., 1998, SSRv, 85, 161
Hachisuka K., Brunthaler A., Menten K. M., Reid M. J., Imai H., et al., 2006, ApJ, 645, 337
Ikeda M., Ohishi M., Nummelin A., Dickens J. E., Bergman P., et al., 2001, ApJ, 560, 792
Jura M., York D. G., 1978, ApJ, 219, 861
Kalenskii S. V., Johansson L. E. B., 2010, ARep, 54, 1084
Kanata H., Yamamoto S., Saito S., 1988, JMoSp, 131, 89
Kawaguchi K., Saito S., Hirota E., 1983, J. Chem. Phys.
Koo B.-C., Lee Y.-H., Moon D.-S., Yoon S.-C., Raymond J. C., 2013, Science, 342, 1346
Liu S.-Y., Mehringer D. M., Snyder L. E., 2001, ApJ, 552, 654
Lykke J. M., Favre C., Bergin E. A., Jørgensen J. K., 2015, A&A, 582, A64
Maciá E., Hernández M. V., Oró J., 1997, OrLi, 27, 459
Marseille M. G., van der Tak F. F. S., Herpin F., Wyrowski F., Chavarría L., et al., 2010, A&A, 521, L32
Matthews H. E., Feldman P. A., Bernath P. F., 1987, ApJ, 312, 358
Millar T. J., Bennett A., Herbst E., 1987, MNRAS, 229, 41P
Ossenkopf V., Henning T., 1994, A&A, 291, 943
Pasek M. A., Lauretta D. S., 2005, AsBio, 5, 515
Qin S.-L., Schilke P., Wu J., Wu Y., Liu T., et al., 2015, ApJ, 803, 39
Remijan A., Snyder L. E., Liu S.-Y., Mehringer D., Kuan Y.-J., 2002, ApJ, 576, 264
Roederer I. U., Jacobson H. R., Thanathibodee T., Frebel A., Toller E., 2014, ApJ, 797, 69
Scott P. F., 1978, MNRAS, 183, 435
Sutton E. C., Blake G. A., Masson C. R., Phillips T. G., 1985, ApJS, 58, 341
Tenenbaum E. D., Woolf N. J., Ziurys L. M., 2007, ApJ, 666, L29
Thorne L. R., Anicich V. G., Prasad S. S., Huntress, Jr. W. T., 1984, ApJ, 280, 139
Turner B. E., Bally J., 1987, ApJ, 321, L75
Vasyunin A. I., Herbst E., 2013, ApJ, 762, 86
Wakelam V., Herbst E., 2008, ApJ, 680, 371
Wilner D. J., Welch W. J., Forster J. R., 1995, ApJ, 449, L73
Wyrowski F., Schilke P., Walmsley C. M., Menten K. M., 1999, ApJ, 514, L43
Xu Y., Reid M. J., Menten K. M., Brunthaler A., Zheng X. W., et al., 2009, ApJ, 693, 413
Zapata L. A., Rodríguez-Garza C., Rodríguez L. F., Girart J. M., Chen H.-R., 2011, ApJ, 740, L19
Zhang Q., Ho P. T. P., 1997, ApJ, 488, 241
Zhang Q., Ho P. T. P., Ohashi N., 1998, ApJ, 494, 636
Ziurys L. M., Friberg P., 1987, ApJL, 314, L49